SLEEP, 2022, 1–9

https://doi.org/10.1093/sleep/zsac178
Advance Access Publication Date: 23 July 2022
Original Article

ORIGINAL ARTICLE

Frontal grey matter microstructure is associated with sleep slow waves characteristics in late midlife

Daphne Chylinski[1], Justinas Narbutas[1,2], Evelyne Balteau[1], Fabienne Collette[1,2], Christine Bastin[1,2], Christian Berthomier[3], Eric Salmon[1,2,4], Pierre Maquet[1,4], Julie Carrier[6,7], Christophe Phillips[1,5], Jean-Marc Lina,[6,7], Gilles Vandewalle[1,*,#] and Maxime Van Egroo[1,8,*,#]

[1]GIGA-Cyclotron Research Centre-In Vivo Imaging, University of Liège, Liège, Belgium, [2]Psychology and Cognitive Neuroscience Research Unit, University of Liège, Liège, Belgium, [3]Physip SA, Paris, France, [4]Department of Neurology, University Hospital of Liège, Liège, Belgium, [5]GIGA-In Silico Medicine, University of Liège, Liège, Belgium, [6]CARSM, CIUSSS of Nord-de l'Île-de-Montréal, Montreal, Canada, [7]Department of Psychology, University of Montreal, Canada and [8]Faculty of Health, Medicine and Life Sciences, School for Mental Health and Neuroscience, Alzheimer Centre Limburg, Maastricht University, Maastricht, The Netherlands

[#]Shared senior authorship.

*Corresponding authors. Gilles Vandewalle, GIGA-Cyclotron Research Centre-In Vivo Imaging, Bâtiment B30, Université de Liège, Allée du Six Août, 8, 4000 Liège, Belgium. Email: gilles.vandewalle@uliege.be; Maxime Van Egroo, Faculty of Health, Medicine and Life Sciences, School for Mental Health and Neuroscience, Alzheimer Centre Limburg, Maastricht University, Universiteitssingel 40, 6229 ER Maastricht, Maastricht, The Netherlands. Email: m.vanegroo@maastrichtuniversity.nl.

Abstract

Study Objectives: The ability to generate slow waves (SW) during non-rapid eye movement (NREM) sleep decreases as early as the 5th decade of life, predominantly over frontal regions. This decrease may concern prominently SW characterized by a fast switch from hyperpolarized to depolarized, or down-to-up, state. Yet, the relationship between these fast and slow switcher SW and cerebral microstructure in ageing is not established.

Methods: We recorded habitual sleep under EEG in 99 healthy late midlife individuals (mean age = 59.3 ± 5.3 years; 68 women) and extracted SW parameters (density, amplitude, frequency) for all SW as well as according to their switcher type (slow vs. fast). We further used neurite orientation dispersion and density imaging (NODDI) to assess microstructural integrity over a frontal grey matter region of interest (ROI).

Results: In statistical models adjusted for age, sex, and sleep duration, we found that a lower SW density, particularly for fast switcher SW, was associated with a reduced orientation dispersion of neurites in the frontal ROI ($p = 0.018$, $R^2_{\beta^*} = 0.06$). In addition, overall SW frequency was positively associated with neurite density ($p = 0.03$, $R^2_{\beta^*} = 0.05$). By contrast, we found no significant relationships between SW amplitude and NODDI metrics.

Conclusions: Our findings suggest that the complexity of neurite organization contributes specifically to the rate of fast switcher SW occurrence in healthy middle-aged individuals, corroborating slow and fast switcher SW as distinct types of SW. They further suggest that the density of frontal neurites plays a key role for neural synchronization during sleep.

Trial registration number: EudraCT 2016-001436-35.

Statement of Significance

Previous studies have evidenced relationships between the age-related changes in grey matter integrity, such as cortical volume or thickness, and alterations in sleep. Slow waves (SW) are among the most commonly impacted features of sleep, their density were reported as reduced in ageing, particularly for SW with a faster down-to-up state transition. Here, we show that neurite characteristics such as their density and organization complexity, are associated with SW parameters, particularly their most fragile form with respect to ageing. Future studies should establish whether preserved neurite content would protect against the neuropathological processes related to Alzheimer's disease through its positive impact on sleep SW, and would ultimately constitute a positive factor in successful cognitive ageing.

Key words: slow waves; fast switcher slow wave; diffusion-weighted imaging; brain microstructure; frontal cortex; NODDI; neurite density; neurite orientation dispersion; ageing

Submitted: 24 March, 2022; **Revised:** 13 July, 2022

Introduction

Human ageing is associated with marked changes in the regulation of sleep and wakefulness [1], that are detected as early as in the 5th decade of life [2, 3]. These changes predict the risk of incident dementia [4] and contribute to the increased prevalence of sleep complaints and insomnia disorder reported in ageing [5, 6]. At the electroencephalographic (EEG) level, various features of sleep slow waves (SW), a gold standard marker of sleep pressure reflecting neuronal synchronization, are notably affected in older individuals [7], as reflected by the reduced density and amplitude of SW, smoother SW slope, and increased duration of the down and up states [3]. These age-related changes are most prominent over the frontal lobe [3], which is particularly involved in the generation of SW [8, 9] and shows high sensitivity to prior sleep-wake history [10]. Though SW are most often considered as a whole, their heterogeneity is now well established [11]. Recently, work by Bouchard and colleagues proposed a novel objective criterion to distinguish SW types based on the frequency of the transition from the hyperpolarized, down state, to the depolarized, up state, differentiating thus so-called slow, and fast switchers [12]. Slow and fast switchers therefore refer to two types of SW that are present in all individuals. The interest of the transition frequency resides in part in the fact that, unlike the slope [13], it is independent of the amplitude of the SW. Critically, they found that the decrease in SW density observed in ageing was most prominent for the fast switchers SW compared with the slow switcher SW, but brain correlates of fast and slow switcher SW in ageing are still lacking.

Age-related changes in sleep–wake regulation have been associated with widespread alterations in brain macrostructure [14]. Accordingly, several cross-sectional studies indicated relationships between the age-related differences in grey matter (GM) integrity measures, such as cortical volume or thickness, and sleep–wake parameters either as self-reports [15] or objective EEG [8, 16, 17] and actigraphy [18] metrics. In longitudinal protocols, these indices have in turn been reported to predict higher rates of GM deterioration [19, 20], suggesting bidirectional detrimental influences between the alterations in brain macrostructure and impaired sleep quality [21].

Recent advances in magnetic resonance imaging (MRI) have provided new means to investigate the age-related changes in brain tissue microstructure in vivo. Among them, the neurite orientation dispersion and density imaging (NODDI) is a multi-compartment diffusion-weighted model which, by discriminating between diffusion signal originating from intracellular, extracellular, and isotropic diffusion [22], enables the investigation of microstructural features within the cortex [23, 24] thanks to quantitative indices probing neurite density (NDI) and their orientation dispersion (ODI).

Here, we recorded habitual sleep via EEG and acquired NODDI data in a large sample of healthy individuals aged 50–69 years (N = 99; 59.3 ± 5.3 years; 68 women). We computed the average characteristics of all SW produced during NREM sleep over the frontal cortex, including the density, the peak-to-peak amplitude, and overall frequency, but also according to whether SW were of the fast or slow switcher type. We further extracted the NDI and ODI values over a set of frontal GM regions critically involved in the generation and the propagation of sleep SW. We hypothesized that, beyond a potential link with age with our limited age-rage sample, higher density, and orientation dispersion of neurites, indicative of a preserved microstructural integrity, would be associated with preserved SW characteristics, i.e. higher density and peak-to-peak amplitude, particularly for the fast switcher SW.

Methods

Study design and participants

One hundred and one healthy older individuals aged 50–70 were enrolled between June, 15th 2016 and October, 2nd 2019 for a multi-modal cross-sectional study taking place at the GIGA-Cyclotron Research Centre/In Vivo Imaging of the University of Liège (Cognitive fitness in ageing—COFITAGE—study; EudraCT: 2016-001436-35). Two participants were excluded from the analyses, due to technical issues with the MRI and sleep data, respectively; leaving 99 individuals for analyses (mean age = 59.3 ± 5.3 years; 68 women; Table 1). All participants were devoid of clinical symptoms of cognitive impairment, as verified by dementia rating scale scores > 130 and mini mental state examination scores > 27. Other exclusion criteria were: body mass index ≤ 18 and ≥ 29; recent (< 10 years) psychiatric history or severe brain trauma; addiction, chronic medication affecting the central nervous system; hypertension; smoking, excessive alcohol (> 14 units/week) or caffeine (> 5 cups/day) consumption; anxiety, as measured by the 21-item self-rated Beck Anxiety Inventory (BAI ≥ 17) [25]; depression, as assessed by the 21-item self-rated Beck Depression Inventory (BDI ≥ 17) [26]. Participants with stable treatment (> 6 months) for hypertension and/or hypothyroidism were included in the study. Individuals with sleep apnea (apnea-hypopnea index ≥ 15/h) were excluded following an in-lab adaptation and screening night of polysomnography. All participants gave their written informed consent and received a financial compensation. This study was approved by the Ethics Committee of the Faculty of Medicine at the University of Liège, Belgium.

Magnetic resonance imaging acquisition

All MRI data were acquired on a 3 T whole-body Magnetom Prisma scanner (Siemens, Erlangen, Germany), with a 64-channel head coil. Diffusion-weighted (DW) data were acquired using a spin-echo echo-planar imaging sequence with a 2 mm isotropic spatial resolution. Acquisition parameters included: TR = 7900 ms, TE = 69 ms, 70 transverse slices, slice thickness = 2 mm, in-plane resolution 2 × 2 mm^2 (field of view = 192 × 216 mm^2, matrix = 96 × 106) and acceleration factor 2, bandwidth per pixel = 2170 Hz/Px. The multi-shell DW imaging (DWI) scheme included 118 volumes. The acquisition time on our Tim-Trio 3T Prisma scanner was exactly 15 min and 57 s. The first volume was discarded to avoid T1 saturation effect. The remaining 117 volumes correspond to a total of 105 DW images interleaved with 12 b = 0 images. The set of diffusion directions was created using electrostatic repulsion [27] and is defined over three shells (b = 650, 1000 and 2000 s/mm^2). Five additional b = 0 volumes with identical acquisition parameters but inverted phase encoding direction were acquired for the estimation of susceptibility-induced distortions. In addition to DW data, a structural quantitative multi-parameter protocol (1 mm^3 voxel size) was acquired and used to generate magnetization transfer

saturation (MTsat) maps as previously described [28] for subsequent data segmentation and normalization.

Magnetic resonance imaging processing

The MRI processing pipeline is summarized and illustrated in Figure 1. For each individual, the MTsat map was segmented into tissue class maps of GM, white matter (WM), and cerebrospinal fluid (CSF) posterior probability using Unified Segmentation [29]. The individual posterior GM and WM maps were then diffeomorphically registered to a study-specific template created with DARTEL [30], and normalized to the Montreal Neurological Institute (MNI) space using DARTEL-estimated individual deformation fields. For DW data, susceptibility-induced, and eddy current-induced distortions, as well as participant's movements, were first estimated, and corrected using *topup* [31] and *eddy* [32] in FSL 5.0.9. Whole-brain NODDI parameter maps (NDI, ODI) were then computed using the Microstructure Diffusion Toolbox [33] (v1.2.6, https://github.com/robbert-harms/MDT). The NDI and ODI maps were registered to the MTsat map and brought into the MNI space by applying normalization parameters estimated previously. Smoothing of normalized NODDI maps was further performed using a tissue-specific weighting which accounts for the partial volume distribution of both GM and WM tissues in each voxel [34], with a full-width at half maximum kernel of 6 mm isotropic.

The region of interest (ROI) was defined as a set of frontal regions commonly involved in studies of sleep SW [35–39]. Based on regions from the Automated Anatomical Labeling atlas (AAL2) [40], we built a composite mask including, bilaterally, medial prefrontal, medial orbito-frontal, dorsolateral frontal, insula, and anterior cingulate cortices. For each individual, the median values of NDI and ODI signals were obtained by applying the ROI on the normalized GM-weighted smoothed NODDI maps. While not completely eliminating potential partial volume effects, this GM-specific processing pipeline aimed at investigating cortical microstructure after removing unwanted contributions from WM and/or CSF to diffusion signal in each voxel. The median of the NDI/ODI over the ROI was chosen as a more robust way of reducing the impact of potential outlier values that might still be present due to partial volume effects or due to the slightly dilated aspect of the atlas used.

Sleep EEG acquisition and processing

As part of the screening process, participants first performed an in-lab adaptation and screening night to minimize the disrupting effect caused by sleeping in a novel environment [41]. Then, for 7 days prior to the baseline night, participants followed a regular sleep–wake schedule (± 30 min), in agreement with their preferred bed and wake-up times. Compliance was verified using sleep diaries and wrist actigraphy (Actiwatch©, Cambridge Neurotechnology, UK). Aside from the fixed sleep-wake schedule, participants were also instructed to abstain from naps, as well as unusually intense physical exercise for the last 3 days of fixed-schedule circadian entrainment. Their habitual sleep was then recorded in complete darkness under EEG. Sleep EEG data were acquired using N7000 amplifiers (EMBLA, Natus Medical Incorporated, Planegg, Germany). The electrode montage consisted of 11 EEG channels (F3, Fz, F4, C3, Cz, C4, P3, Pz, P4, O1, O2), 2 bipolar EOGs, and 2 bipolar EMGs. The signal was re-referenced to the average of both mastoids. Scoring of

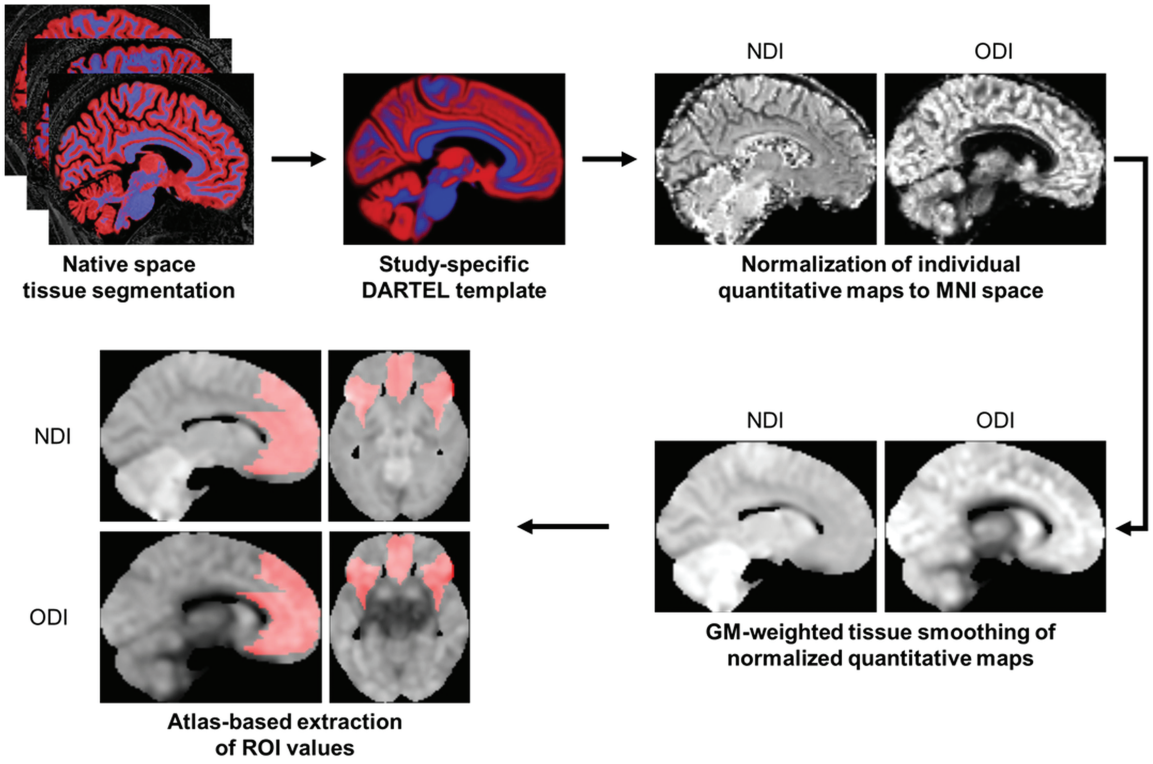

Figure 1. Summary illustration of the MRI processing pipeline. Refer to the text for details.

baseline night in 30-s epochs was performed automatically using a validated algorithm (ASEEGA, PHYSIP, Paris, France) [42, 43]. An automatic detection algorithm with adapting thresholds was further applied to exclude artifacts and arousals from the scored data [44, 45]

SW were automatically detected on N2 and N3 epochs free of artifacts > 5 s, via a previously developed algorithm [46]. First, data were band-filtered between 0.3 and 4 Hz with a linear phase finite impulse response filter. Based on recent work [46], the SW detection criteria were adapted for age and sex [46]: instead of the standard ≥ 75 μV peak-to-peak amplitude and ≥ -40 μV for the negative peak, the thresholds were lowered to ≥ 70 μV and ≥ -37 μV for women, and ≥ 60.5 μV and ≥ -32 μV for men. The duration of the negative deflection ranged between 125 and 1500 ms, and the duration of the positive deflection had to fit below 1000 ms. For all SW corresponding to the aforementioned criteria, the following parameters were extracted over the frontal electrodes (F3-Fz-F4): SW density, computed as the number of SW per minute of N2/N3 sleep; SW amplitude, corresponding to the amplitude in μV from the down-to the up state; and SW frequency, corresponding to the inverse of the total duration of the SW, a measure that is independent of SW amplitude. After being computed for each of the three frontal electrodes separately, those parameters were then averaged. As described elsewhere [12], SW were sorted according to their down-to-up state transition frequency into either slow (< 1.2 Hz) or fast switchers (≥ 1.2 Hz) SW. SW parameters (SW density, amplitude, and frequency) were also computed for those two types of SW separately. Slow and fast switchers refer to two types of SW that are present in all individuals.

Statistics

Statistical analyses were performed using Generalized Linear Mixed Models (GLMMs) in SAS 9.4 (SAS Institute, Cary, NC). For each statistical model, the distribution of the dependent variable was first determined in MATLAB and the GLMMs were adjusted accordingly. All GLMMs with SW characteristics as dependent variable included fixed effects for NODDI metric (either median ROI NDI or median ROI ODI), age, sex, as well as total sleep time (TST), while subject (intercept) was included as a random effect. Statistical significance was set at $p < 0.05$. Statistical models were first performed considering all SW, i.e. regardless of their down-to-up state transition frequency. When analyses indicated a significant result or a statistical trend ($p < 0.10$), analyses were further carried out per SW switcher (slow/fast) type. Degrees of freedom in GLMMs were estimated using Kenward-Roger's correction. Semi-partial R^2 ($R^2_{\beta^*}$) values were computed to estimate the effect size of significant fixed effects in all GLMMs [47].

Optimal sensitivity and power analyses in GLMM remain under investigation [e.g [48].]. We nevertheless computed an a priori sensitivity analysis to get an indication of the minimum detectable effect size in our main analyses given our sample size. According to G*Power 3 (version 3.1.9.4) [49] taking into account a power of .8, an error rate α of .05, a sample size of 99 allowed us to detect small effect sizes $r > .27$ (2-sided; absolute values; confidence interval: .076–.44; $R^2 > .07$, R^2 confidence interval: .005–.19) within a linear multiple regression framework including 1 tested predictor (NODDI metric) and 3 covariates (age, sex, TST).

Results

We first assessed the effect of age on both NODDI parameters over the frontal ROI using GLMMs adjusted for sex. We found that NDI was not significantly associated with age ($F_{1,96} = 1.64$, $p = 0.2$), or sex ($F_{1,96} = 2.2$, $p = 0.14$). ODI, on the other hand, showed a significant, negative relationship with age ($F_{1,96} = 14.89$, $p = 0.0002$), but not with sex ($F_{1,96} = 1.58$, $p = 0.21$) (Figure 2). In our 50-to-69-years sample, the index of neurite density is therefore not significantly associated with age, while neurite orientation dispersion or diversity significantly decreases with age. In the associations with SW characteristics, we therefore focused on the ODI metric prior to exploratory analyses using the NDI metric.

Neurite orientation dispersion (ODI)

In a first GLMM, we found a statistical trend for a positive relationship between median ODI values over frontal regions (Figure 3a) and SW density ($F_{1,94} = 3.75$, $p = 0.056$, $R^2_{\beta^*} = 0.04$, Figure 3b),

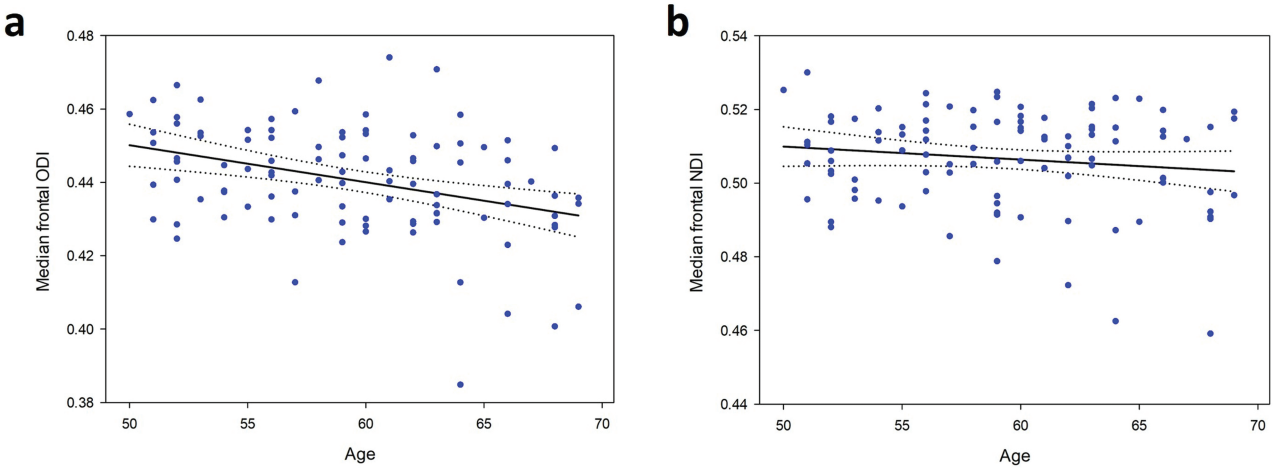

Figure 2. Associations between age and median frontal ODI values (a) and the median frontal NDI values (b). Simple regressions were used only for a visual display and do not substitute the GLMM outputs.

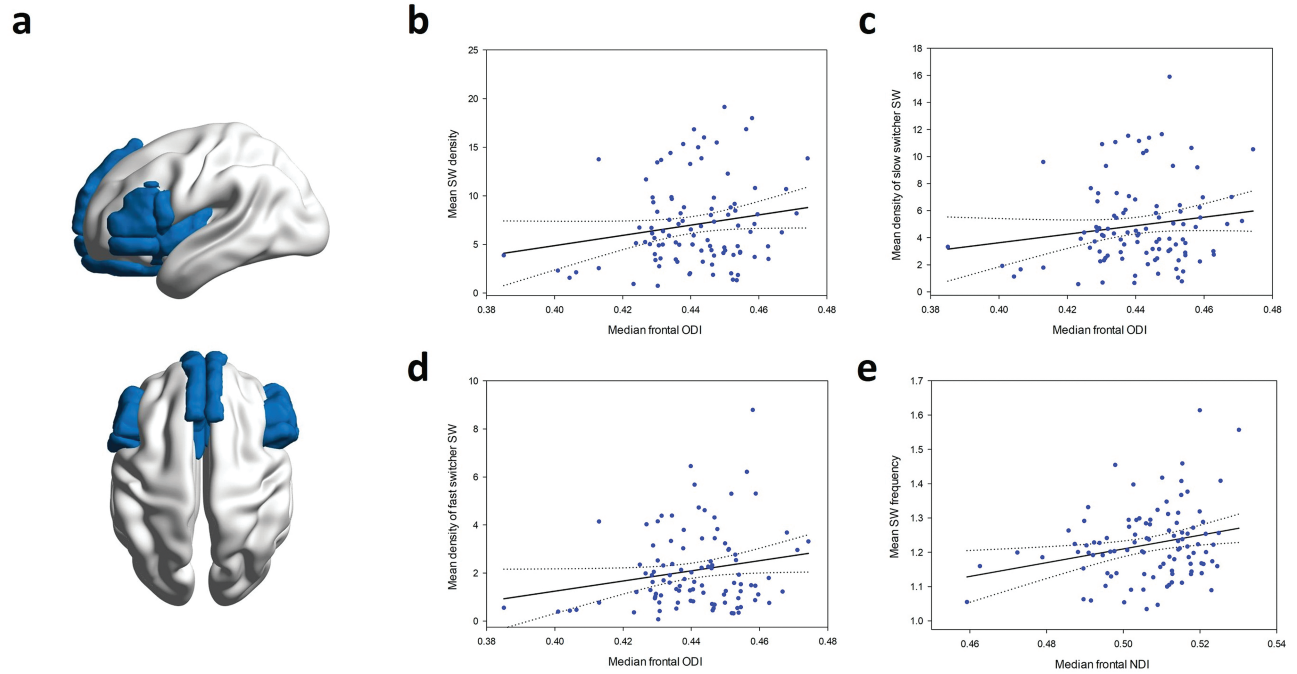

Figure 3. Relationships between slow wave characteristics and frontal ROI NDI and ODI metrics. (a) NODDI metrics were obtained for a set of frontal cortical regions highlighted here. (b) Positive association between ODI and mean slow wave density ($p = 0.056$). (c) No significant association between ODI and slow switcher SW density ($p = 0.13$). (d) Significant positive association between ODI and fast switcher SW density ($p = 0.018$). (e) Positive association between NDI and mean slow wave frequency ($p = 0.03$). Simple regressions were used only for a visual display and do not substitute the GLMM outputs.

on top of a significant effect of sex, while no effect of age or TST was found (Table 2). Given the trend for a link between SW density and ODI values, we examined if the median ODI values would be selectively associated with a specific type of SW (slow or fast switchers). We found a significant association between the density of fast switcher SW and median ODI values ($F_{1,94} = 5.82$, $p = 0.018$, $R^2_{\beta^*} = 0.06$, Figure 3d), but not for the density of slow switcher SW ($F_{1,94} = 2.36$, $p = 0.13$) (Figure 3c). In a GLMM with SW amplitude as the dependent variable, we observed no link with median ODI values ($F_{1,94} = 0.23$, $p = 0.64$) nor TST but an effect of age and sex (Table 2). Regarding the SW frequency, we found no significant relationship with median ODI ($F_{1,94} = 0.94$, $p = 0.33$), and no effect of age, sex, or TST (Table 2).

Neurite density (NDI)

In a set of exploratory GLMMs, we then considered the NDI metric. We assessed whether SW density was associated with NDI in the frontal ROI, while controlling for age, sex, and TST. We found no significant association between SW density and median NDI values ($F_{1,94} = 1.51$, $p = 0.22$), but, in line with the literature [3], a significant negative link between SW density and age, as well as an effect of sex, with lower SW density in men (Table 3). A similar pattern was observed for SW amplitude, for which we found no significant association with median NDI values ($F_{1,94} = 1.36$, $p = 0.25$), but an expected [50] significant negative relationship with age, and sex with, again, lower values in men (Table 3). By contrast, a GLMM with the SW frequency as dependent variable revealed a significant positive association with median NDI values ($F_{1,94} = 4.64$, $p = 0.03$, $R^2_{\beta^*} = 0.05$, Figure 2e), but no significant effect of age, sex, or TST (Table 3). Given this result, we aimed to explore if this relationship was driven by a specific type of SW (slow or fast switchers), but we found no significant relationship between the overall frequency of a specific SW type and NDI values (slow switchers: $F_{1,94} = 3.22$, $p = 0.07$; fast switchers $F_{1,94} = 2.12$, $p = 0.15$; Table 3).

Discussion

Physiological ageing is inherently accompanied by modifications in brain structure that are associated with a disruption of the regulation of sleep and wakefulness, most likely in a bidirectional manner [21, 51]. Expanding on previous studies which focused on macrostructural measures of brain structural integrity to investigate the neurobiological correlates of the age-related decrease in NREM sleep SW generation [8, 17, 38, 39], we tested whether brain tissue microstructural properties as assessed in vivo with the NODDI biophysical model could be associated with SW characteristics in a sample of healthy late midlife individuals aged 50–69 years. Importantly, in addition to the density, amplitude, and overall frequency of the SW, we also characterized the SW according to their down-to-up state transition frequency. We first found that a lower orientation dispersion of neurites over a frontal cortex ROI, as measured with the ODI metric, was linked to a lower density of fast switcher SW. This finding lends support to the validity of using the down-to-up state transition frequency to meaningfully separate different types of SW, and provides brain correlates of the previously reported greater impact of ageing on the fast switcher SW [12]. In addition, we report that a higher neurite density over the same frontal ROI, as reflected in the NDI values, was associated with a higher overall frequency of the SW.

Changes in the concentrations of neuromodulators associated with NREM sleep lead neurons to spontaneously alternate

Table 1. Demographic characteristics of the study sample (mean ± SD [range])

Sex	68 ♀/31 ♂
Age (years)	59.3 ± 5.3 [50–69]
Education (years)	15.2 ± 3.0 [9–25]
Total sleep time (TST) (min, EEG)	393.1 ± 47.0 [229–495.5]
Time spent in sleep stage (% of TST, EEG)	
N1	6.2 ± 2.8 [0.6–15.6]
N2	51.3 ± 8.7 [31.4–75.7]
N3	19.1 ± 6.5 [7.2–38.3]
REM	23.3 ± 6.8 [6.5–39.8]
Mean SW density (number/minute of N2/N3)	
All slow waves	7.1 ± 4.3 [0.8–19.2]
Slow switchers	4.9 ± 3.1 [0.6–15.9]
Fast switchers	2.1 ± 1.6 [0.1–8.8]
Mean SW amplitude (μV)	
All slow waves	101.6 ± 12.4 [76.0–128.2]
Slow switchers	104.7 ± 13.7 [77.7–131.3]
Fast switchers	94.1 ± 11.0 [73.0–130.1]
Mean frequency	
All slow waves	1.2 ± 0.1 [1.0–1.6]
Slow switchers	1.1 ± 0.1 [1.0–1.3]
Fast switchers	1.5 ± 0.1 [1.3–1.8]
Mean transition frequency	
All slow waves	1.4 ± 0.1 [1.1–1.8]
Slow switchers	1.1 ± 0.0 [1.0–1.2]
Fast switchers	2.0 ± 0.1 [1.9–2.2]
Median ROI values	
NDI	0.51 ± 0.01 [0.46–0.53]
ODI	0.44 ± 0.01 [0.38–0.47]

NDI, neurite density index; *ODI*, neurite orientation dispersion index; *ROI*, region of interest; *SW*, slow waves; *TST*, total sleep time.

Table 2. Outputs of GLMMs performed on ODI values (one row represents one model)

	Age	Sex	TST	ODI
SW density	$F = 2.41$	**$F = 13.39$**	$F = 0.68$	$F = 3.75$
	$p = 0.12$	**$p = 0.0004$**	$p = 0.41$	$p = 0.056$
		$R^2\beta^* = 0.12$		$R^2_{\beta^*} = 0.04$
Slow switchers density	$F = 1.83$	**$F = 9.31$**	$F = 0.37$	$F = 2.36$
	$p = 0.18$	**$p = 0.003$**	$p = 0.55$	$p = 0.13$
		$R^2\beta^* = 0.09$		
Fast switchers density	$F = 2.88$	**$F = 18.59$**	$F = 1.05$	**$F = 5.82$**
	$p = 0.09$	**$p < 0.0001$**	$p = 0.31$	**$p = 0.018$**
		$R^2\beta^* = 0.17$		**$R^2\beta^* = 0.06$**
SW amplitude	**$F = 8.62$**	**$F = 148.93$**	$F = 2.62$	$F = 0.23$
	$p < 0.0001$	**$p < 0.0001$**	$p = 0.11$	$p = 0.64$
	$R^2\beta^* = 0.08$	**$R^2\beta^* = 0.61$**		
SW frequency	$F = 0.52$	$F = 3.69$	$F = 0.00$	$F = 0.94$
	$p = 0.47$	$p = 0.06$	$p = 0.99$	$p = 0.33$

Degrees of freedom for all the aforementioned models are 1 (numerator) and 94 (denominator). Bold values indicate significant effects ($p < 0.05$).
ODI, neurite orientation dispersion index; *SW*, slow waves; *TST*, total sleep time.

Table 3. Outputs of GLMMs performed on NDI values (one row represents one model)

	Age	Sex	TST	NDI
SW density	**$F = 4.88$**	**$F = 10.57$**	$F = 0.32$	$F = 1.51$
	$p = 0.030$	**$p = 0.0016$**	$p = 0.58$	$p = 0.22$
	$R^2\beta^* = 0.05$	**$R^2\beta^* = 0.10$**		
SW amplitude	**$F = 9.77$**	**$F = 138.51$**	$F = 3.48$	$F = 1.36$
	$p = 0.002$	**$p < 0.0001$**	$p = 0.07$	$p = 0.25$
	$R^2\beta^* = 0.09$	**$R^2\beta^* = 0.60$**		
SW frequency	$F = 1.01$	$F = 2.53$	$F = 0.23$	**$F = 4.64$**
	$p = 0.32$	$p = 0.12$	$p = 0.64$	**$p = 0.03$**
				$R^2\beta^* = 0.05$
Slow switchers frequency	$F = 0.32$	$F = 1.49$	$F = 0.75$	$F = 3.22$
	$p = 0.57$	$p = 0.23$	$p = 0.39$	$p = 0.076$
Fast switchers frequency	$F = 1.40$	**$F = 4.64$**	$F = 0.03$	$F = 2.12$
	$p = 0.24$	**$p = 0.03$**	$p = 0.85$	$p = 0.15$
		$R^2\beta^* = 0.05$		

Degrees of freedom for all the aforementioned models are 1 (numerator) and 94 (denominator). Bold values indicate significant effects ($p < 0.05$).
NDI, neurite density index; *SW*, slow waves; *TST*, total sleep time.

between down (silent) hyperpolarised, and up (firing) depolarized states [52, 53]. These alternations are synchronized across patches of the cortical tissues generating an electrical signal taking the form of a SW, as measured with the EEG at the level of the scalp. For a given SW, the number of contributing neurons and their relative synchrony influence the amplitude of the detected SW as well as the duration of the down and up states, which in turn determine the overall frequency of the SW. As only those brain oscillations reaching a given amplitude are considered as SW [50, 54], these elements eventually contribute to the density of SW. The latter further depends on the need for SW, which, according to a wealth of literature, reflects the need for sleep [55]. Finally, the synchrony of neuron transition from the down-to the up state will determine the duration of the SW transition from the down-to the up (minimum to maximum value), corresponding to the transition frequency of a SW [12].

The ODI values reflect the coherence in the orientation of neurites within the underlying tissue, a low index indicating completely aligned fibers, while a high index indicates isotropy [56] (i.e. no dominant orientation). In the GM, the ODI thus represents the branching complexity of the neurite trees and can be seen as a marker of GM complexity, with higher isotropy meaning more complexity [22]. Despite the limited age range in our sample, we found that the ODI index decreases as one gets from 50 to 70 years, suggesting that a preserved brain integrity in older individuals is associated with a higher neurite orientation dispersion. In line with this inference, we observed a positive association between ODI values and SW density of fast switchers SW [12]. Our results therefore suggest that microstructural GM complexity may help maintaining the generation of sleep SW, particularly their most fragile form with respect to ageing [12], i.e. fast switcher SW, in the sixth and seventh decades of life. The age-related decrease in the frequency of SW has been speculated to be the consequence of less synchronicity between cortical neurons when entering the hyperpolarized and depolarized states [3, 12]. Our result suggests that the complexity of neurite organization may indeed be related to neuronal synchronization, e.g. by interconnecting a large population of neurons, but particularly so for fast switcher SW. Alternatively, the complexity of the organization of neurites could be related to a higher average synaptic cost that would contribute to a higher need for sleep leading to more fast switchers SW. Given the age-related increase in sleep complaints and insomnia disorders [5, 6], one could speculate that a reduction in the complexity of neurite organization contributes to a less intense

and more fragile sleep characterized by less fast switcher SW. Furthermore, we observe that the density of neurites, as indexed by NDI values, was positively associated with the mean frequency of the SW, irrespective of the slow of fast switcher type and beyond the effect age could have on the latter. This suggests that in healthy late midlife, a higher density of neurites would tighten the overall bounds between the neurons and promote their synchrony when entering down and up states. Our study does not indicate, at least not in healthy and relatively young older adults, that the density of neurites is linked to the density of SW. Thus, it is possible that the mere number of neurite connections within the GM tissue may not be related to the need for sleep, at least much less so than to the synchrony of SW.

Our study includes a relatively large sample of thoroughly screened healthy late midlife individuals. This means that, compared to the general population, the variability in the NODDI and SW parameters was likely reduced in our sample. Yet, we were still able to isolate significant associations between the brain microstructure indices and SW characteristics. The fact that the computed brain microstructure indices were based on state-of-the-art MRI data acquisition and processing approaches [57, 58] most probably contribute to isolating the effects. This limited variability could, however, only yield small statistical effect sizes, warranting replication in larger or more diverse samples. Moreover, whereas the literature strongly supports the involvement of frontal regions in age-related changes, both with regards to the structural integrity of the brain and to sleep SW, the regional aspect of the relationships highlighted here should be extended to the whole-brain. As deep pyramidal cells provide most of the recorded EEG signal at the electrode level [59] and seem to play an important role in sleep homeostasis [60], characterizing NODDI parameters within cortical layers would refine our understanding of the complex link between microstructural integrity and the synchronized activity among neuronal populations, but the spatial resolution inherent to currently available DWI sequences constitutes an important obstacle to do so in vivo. It would also be of prime interest to conduct a longitudinal study to assess more thoroughly whether the individual trajectories of changes in brain microstructure are related to the maintenance of SW characteristics.

An increasing body of evidence shows that the quality of sleep and wakefulness regulation is crucial to sustain cognition in normal and pathological ageing [4, 61, 62]. The quantification of NREM sleep SW has been associated with a higher amyloid-beta (Aβ) burden in the medial prefrontal cortex [37], a hallmark of Alzheimer's disease (AD) neuropathology, while the experimental reduction of sleep SW increases Aβ content in the CSF [63]. It is therefore tempting to speculate, based on the current findings, that a preserved neurite content would protect against the neuropathological AD-related processes through its positive impact on sleep SW, and would ultimately constitute a positive factor in successful cognitive ageing. These effects should be more pronounced and of greater magnitude in neurodegenerative and/or sleep disorders that are associated with marked alterations in both brain and sleep measures. The first steps to test this speculation would be to assess regional NODDI parameters in preclinical AD patients (Mild Cognitive Impairment—MCI) and in AD patients or to investigate whether NODDI parameters are associated with regional Aβ or tau burden in healthy individual or patients as suggested in animal studies [64], and whether it could be linked to cognition in older individuals. Interestingly, manipulation of SW overall frequency was recently related to Aβ production in mice [65]. The regional burden of the other key hallmark of AD neuropathology, the accumulation of tau protein neurofibrillary tangles, also deserves further investigations [66].

In summary, our cross-sectional study shows that, in healthy late midlife, brain microstructural metrics related to the density of neurites and their orientation dispersion, as measured over the medial and dorsolateral frontal cortex, are associated with the preserved ability to generate SW during NREM and do so through synchronous neuronal activity. These findings may have implications for successful ageing, insomnia, and neurodegenerative diseases.

Acknowledgments

We thank M. Blanpain, P. Cardone, M. Cerasuolo, E. Lambot, C. Hagelstein, S. Laloux, A. Claes, C. Degueldre, B. Herbillon, P. Hawotte, B. Lauricella, A. Lesoine, A. Luxen, X. Pepin, E. Tezel, D. Marzoli, C. Schmidt and P. Villar González for their help in different steps of the study. This work was supported by Fonds National de la Recherche Scientifique (FRS-FNRS, FRSM 3.4516.11, Belgium), Actions de Recherche Concertées (ARC SLEEPDEM 17/27-09) of the Fédération Wallonie-Bruxelles, University of Liège (ULiège), European Regional Development Fund (ERDF, Radiomed Project), Fondation Recherche Alzheimer – SAO-FRA Belgium, and the Canadian Institutes of Health Research (CIHR) (grant number 190750). M.V.E. is supported by BrightFocus Foundation (A20211016F) and was supported by the F.R.S.-FNRS Belgium and Wallonia-Brussel International (WBI). C.Bastin, F.C., C.P., and G.V. are supported by the F.R.S.-FNRS Belgium. C. Berthomier, is the owner of Physip, the company that analyzed the EEG data as part of a collaboration. This ownership and the collaboration had no impact on the design, data acquisition and interpretations of the findings

Disclosure Statement

Financial disclosure: none. Non-financial disclosure: none.

Author Contributions

Study concept and design: D.C., M.V.E., E.S., P.M., C.P., C.Bastin, F.C. and G.V. Data acquisition: D.C., M.V.E. J.N., V.M., C.Bastin, F.C., G.V. Data analysis and interpretation: all authors. D.C., G.V. and M.V.E. drafted the first version of the manuscript. All authors revised the manuscript and had final responsibility for the decision to submit for publication.

Data Availability

The data underlying this article will be shared on reasonable request to the corresponding author.

References

1. Mander BA, *et al.* Sleep and human aging. *Neuron.* 2017;**94**(1):19–36. doi:10.1016/j.neuron.2017.02.004.

2. Cajochen C, *et al*. Age-related changes in the circadian and homeostatic regulation of human sleep. *Chronobiol Int*. 2006;**23**(1–2):461–474. doi:10.1080/07420520500545813.
3. Carrier J, *et al*. Sleep slow wave changes during the middle years of life. *Eur J Neurosci*. 2011;**33**(4):758–766. doi:10.1111/j.1460-9568.2010.07543.x.
4. Shi L, *et al*. Sleep disturbances increase the risk of dementia: a systematic review and meta-analysis. *Sleep Med Rev*. 2018;**40**:4–16. doi:10.1016/j.smrv.2017.06.010.
5. Robbins R, *et al*. Sleep difficulties, incident dementia and all-cause mortality among older adults across 8 years: findings from the National Health and Aging Trends Study. *J Sleep Res*. 2021;**30**(6):1–10. doi:10.1111/jsr.13395.
6. Morin CM, *et al*. Epidemiology of insomnia: prevalence, self-help treatments, consultations, and determinants of help-seeking behaviors. *Sleep Med*. 2006;**7**(2):123–130. doi:10.1016/j.sleep.2005.08.008.
7. Léger D, *et al*. Slow-wave sleep: from the cell to the clinic. *Sleep Med Rev*. 2018;**41**:113–132. doi:10.1016/j.smrv.2018.01.008.
8. Dubé J, *et al*. Cortical thinning explains changes in sleep slow waves during adulthood. *J Neurosci*. 2015;**35**(20):7795–7807. doi:10.1523/JNEUROSCI.3956-14.2015.
9. Murphy M, *et al*. Source modeling sleep slow waves. *Proc Natl Acad Sci USA*. 2009;**106**(5):1608–1613. doi:10.1073/pnas.0807933106.
10. Schmidt C, *et al*. Age-related changes in sleep and circadian rhythms: impact on cognitive performance and underlying neuroanatomical networks. *Front Neurol*. 2012;**3**:118. doi:10.3389/fneur.2012.00118.
11. Achermann P, Borbély AA. Low-frequency (< 1 hz) oscillations in the human sleep electroencephalogram. *Neuroscience*. 1997;**81**(1):213–222. doi:10.1016/s0306-4522(97)00186-3
12. Bouchard M, *et al*. Sleeping at the switch. *Elife*. 2021;**10**:e64337. doi:10.7554/eLife.64337.
13. Riedner BA, *et al*. Sleep homeostasis and cortical synchronization: III. A high-density EEG study of sleep slow waves in humans. *Sleep*. 2007;**30**(12):1643–1657. doi:10.1093/sleep/30.12.1643.
14. Baillet M, *et al*. Sleep, rest-activity fragmentation and structural brain changes related to the ageing process. *Curr Opin Behav Sci*. 2020;**33**:8–16. doi:10.1016/j.cobeha.2019.11.003.
15. Carvalho DZ, *et al*. Excessive daytime sleepiness and fatigue may indicate accelerated brain aging in cognitively normal late middle-aged and older adults. *Sleep Med*. 2017;**32**:236–243. doi:10.1016/j.sleep.2016.08.023.
16. Van Someren EJW, *et al*. Medial temporal lobe atrophy relates more strongly to sleep-wake rhythm fragmentation than to age or any other known risk. *Neurobiol Learn Mem*. 2018;**160**(May):132–138. doi:10.1016/j.nlm.2018.05.017.
17. Baril A-A, *et al*. Slow-wave sleep and MRI markers of brain aging in a community-based sample. *Neurology*. 2021;**96**(10):e1462–e1469. doi:10.1212/WNL.0000000000011377.
18. Lim ASP, *et al*. Regional neocortical gray matter structure and sleep fragmentation in older adults. *Sleep*. 2016;**39**(1):227–235. doi:10.5665/sleep.5354.
19. Sexton CE, *et al*. Poor sleep quality is associated with increased cortical atrophy in community-dwelling adults. *Neurology*. 2014;**83**(11):967–973. doi:10.1212/WNL.0000000000000774.
20. Spira AP, *et al*. Sleep duration and subsequent cortical thinning in cognitively normal older adults. *Sleep*. 2016;**39**(5):1121–1128. doi:10.5665/sleep.5768.
21. Van Egroo M, *et al*. Sleep–wake regulation and the hallmarks of the pathogenesis of Alzheimer's disease. *Sleep*. 2019;**42**(4):1–13. doi:10.1093/sleep/zsz017.
22. Zhang H, *et al*. NODDI: practical in vivo neurite orientation dispersion and density imaging of the human brain. *Neuroimage*. 2012;**61**(4):1000–1016. doi:10.1016/j.neuroimage.2012.03.072.
23. Fukutomi H, *et al*. Neurite imaging reveals microstructural variations in human cerebral cortical gray matter. *Neuroimage*. 2018;**182**(May 2017):488–499. doi:10.1016/j.neuroimage.2018.02.017.
24. Gozdas E, *et al*. Neurite imaging reveals widespread alterations in gray and white matter neurite morphology in healthy aging and amnestic mild cognitive impairment. *Cereb Cortex*. 2021;**31**(12):5570–5578. doi:10.1093/cercor/bhab180.
25. Beck AT, *et al*. An inventory for measuring clinical anxiety: psychometric properties. *J Consult Clin Psychol*. 1988;**56**(6):893–897. doi:10.1037/0022-006X.56.6.893.
26. Beck AT, *et al*. Psychometric properties of the beck depression inventory: twenty-five years of evaluation. *Clin Psychol Rev*. 1988;**8**:77–100. doi:10.1016/0272-7358(88)90050-5.
27. Slater DA, *et al*. Evolution of white matter tract microstructure across the life span. *Hum Brain Mapp*. 2019;**40**(7):2252–2268. doi:10.1002/hbm.24522.
28. Van Egroo M, *et al*. Early brainstem [18F]THK5351 uptake is linked to cortical hyperexcitability in healthy aging. *JCI Insight*. 2021;**6**(2):0–13. doi:10.1172/jci.insight.142514.
29. Ashburner J, *et al*. Unified segmentation. *Neuroimage*. 2005;**26**(3):839–851. doi:10.1016/j.neuroimage.2005.02.018.
30. Ashburner J. A fast diffeomorphic image registration algorithm. *Neuroimage*. 2007;**38**(1):95–113. doi:10.1016/j.neuroimage.2007.07.007.
31. Andersson JLR, *et al*. How to correct susceptibility distortions in spin-echo echo-planar images: application to diffusion tensor imaging. *Neuroimage*. 2003;**20**(2):870–888. doi:10.1016/S1053-8119(03)00336-7.
32. Andersson JLR, *et al*. An integrated approach to correction for off-resonance effects and subject movement in diffusion MR imaging. *Neuroimage*. 2016;**125**:1063–1078. doi:10.1016/j.neuroimage.2015.10.019.
33. Harms RL, *et al*. Robust and fast nonlinear optimization of diffusion MRI microstructure models. *Neuroimage*. 2017;**155**(April):82–96. doi:10.1016/j.neuroimage.2017.04.064.
34. Draganski B, *et al*. Regional specificity of MRI contrast parameter changes in normal ageing revealed by voxel-based quantification (VBQ). *Neuroimage*. 2011;**55**(4):1423–1434. doi:10.1016/j.neuroimage.2011.01.052.
35. Dang-Vu TT, *et al*. Cerebral correlates of delta waves during non-REM sleep revisited. *Neuroimage*. 2005;**28**(1):14–21. doi:10.1016/j.neuroimage.2005.05.028.
36. Dang-Vu TT. Neuronal oscillations in sleep: insights from functional neuroimaging. *Neuromolecular Med*. 2012;**14**(3):154–167. doi:10.1007/s12017-012-8166-1.
37. Mander BA, *et al*. β-amyloid disrupts human NREM slow waves and related hippocampus-dependent memory consolidation. *Nat Neurosci*. 2015;**18**(7):1051–1057. doi:10.1038/nn.4035.
38. Saletin JM, *et al*. Structural brain correlates of human sleep oscillations. *Neuroimage*. 2013;**83**:658–668. doi:10.1016/j.neuroimage.2013.06.021.
39. Mander BA, *et al*. Prefrontal atrophy, disrupted NREM slow waves and impaired hippocampal-dependent memory in aging. *Nat Neurosci*. 2013;**16**(3):357–364. doi:10.1038/nn.3324.
40. Tzourio-Mazoyer N, *et al*. Automated anatomical labeling of activations in SPM using a macroscopic anatomical parcellation of the MNI MRI single-subject brain. *Neuroimage*. 2002;**15**(1):273–289. doi:10.1006/nimg.2001.0978.

41. Tamaki M, *et al*. Night watch in one brain hemisphere during sleep associated with the first-night effect in humans. *Curr Biol*. 2016;**26**(9):1190–1194. doi:10.1016/j.cub.2016.02.063.
42. Berthomier C, *et al*. Automatic analysis of single-channel sleep EEG: validation in healthy individuals. *Sleep*. 2007;**30**(11):1587–1595. doi:10.1093/sleep/30.11.1587.
43. Peter-Derex L, *et al*. Automatic analysis of single-channel sleep EEG in a large spectrum of sleep disorders. *J Clin Sleep Med*. 2020;**17**(3):393–402. doi:10.5664/jcsm.8864.
44. Coppieters 't Wallant D, *et al*. Automatic artifacts and arousals detection in whole-night sleep EEG recordings. *J Neurosci Methods*. 2016;**258**:124–133. doi:10.1016/j.jneumeth.2015.11.005.
45. Chylinski D, *et al*. Validation of an automatic arousal detection algorithm for whole-night sleep EEG recordings. *Clocks and Sleep*. 2020;**2**(3):258–272. doi:10.3390/clockssleep2030020.
46. Rosinvil T, *et al*. Are age and sex effects on sleep slow waves only a matter of electroencephalogram amplitude? *Sleep*. 2021;**44**(3):1–12. doi:10.1093/sleep/zsaa186.
47. Jaeger BC, *et al*. An R^2 statistic for fixed effects in the generalized linear mixed model. *J Appl Stat*. 2017;**44**(6):1086–1105. doi:10.1080/02664763.2016.1193725.
48. Kain MP, *et al*. A practical guide and power analysis for GLMMs: Detecting among treatment variation in randomeffects. *PeerJ*. 2015;**2015**(9). doi:10.7717/peerj.1226.
49. Faul F, *et al*. Statistical power analyses using G*Power 3.1: tests for correlation and regression analyses. *Behav Res Methods*. 2009;**41**(4):1149–1160. doi:10.3758/BRM.41.4.1149.
50. Rosinvil T, *et al*. Are age and sex effects on sleep slow waves only a matter of EEG amplitude? *Sleep*. 2020;**44**(3):zsaa186. doi:10.1093/sleep/zsaa186.
51. Van Egroo M, *et al*. Sleep–wake regulation and the hallmarks of the pathogenesis of Alzheimer's disease. *Sleep*. 2019;**42**(4):1–13. doi:10.1093/sleep/zsz017.
52. Steriade M, *et al*. Natural waking and sleep states: a view from inside neocortical neurons. *J Neurophysiol*. 2001;**85**(5):1969–1985. doi:10.1152/jn.2001.85.5.1969.
53. Ding F, *et al*. Changes in the composition of brain interstitial ions control the sleep-wake cycle. *Science*. 2016;**352**(6285):550–555.
54. Iber C, *et al*. *The AASM Manual for the Scoring of Sleep and Associated Events: Rules, Terminology and Technical Specifications*. Westchester, IL: American Academy of Sleep Medicine; 2007.
55. Vyazovskiy VV, *et al*. Electrophysiological correlates of sleep homeostasis in freely behaving rats. *Prog Brain Res*. 2011;**193**(608):17–38. doi:10.1016/B978-0-444-53839-0.00002-8.
56. Kamiya K, *et al*. NODDI in clinical research. *J Neurosci Methods*. 2020;**346**(March):108908. doi:10.1016/j.jneumeth.2020.108908.
57. Tabelow K, *et al*. hMRI—a toolbox for quantitative MRI in neuroscience and clinical research. *Neuroimage*. 2019;**194**(December 2018):191–210. doi:10.1016/j.neuroimage.2019.01.029.
58. Harms RL, *et al*. Robust and fast Markov Chain Monte Carlo sampling of diffusion MRI microstructure models. *Front Neuroinform*. 2018;**12**(December):1–18. doi:10.3389/fninf.2018.00097.
59. Cohen MX. Where does EEG come from and what does it mean? *Trends Neurosci*. 2017;**40**(4):208–218. doi:10.1016/j.tins.2017.02.004.
60. Krone LB, *et al*. A role for the cortex in sleep–wake regulation. *Nat Neurosci*. 2021;**24**(9):1210–1215. doi:10.1038/s41593-021-00894-6.
61. Latreille V, *et al*. Age-related cortical signatures of human sleep electroencephalography. *Neurobiol Aging*. 2019;**76**:106–114. doi:10.1016/j.neurobiolaging.2018.12.012.
62. Djonlagic I, *et al*. Macro and micro sleep architecture and cognitive performance in older adults. *Nat Hum Behav*. 2020;**5**(1):123–145. doi:10.1038/s41562-020-00964-y.
63. Ju YS, *et al*. Slow wave sleep disruption increases cerebrospinal fluid amyloid- b levels. *Brain*. 2017;**140**(November):2104–2111. doi:10.1093/brain/awx148.
64. Colgan N, *et al*. Application of neurite orientation dispersion and density imaging (NODDI) to a tau pathology model of Alzheimer's disease. *Neuroimage*. 2016;**125**:739–744. doi:10.1016/j.neuroimage.2015.10.043.
65. Kastanenka KV, *et al*. Frequency-dependent exacerbation of Alzheimer's disease neuropathophysiology. *Sci Rep*. 2019;**9**(1):1–14. doi:10.1038/s41598-019-44964-z.
66. Vogt NM, *et al*. Interaction of amyloid and tau on cortical microstructure in cognitively unimpaired adults. *Alzheimer's Dement*. 2021;**18**(1):1–2. doi: 10.1002/alz.12364.